Proton Echo-Planar Spectroscopic Imaging of *J*-Coupled Resonances in Human Brain at 3 and 4 Tesla

Stefan Posse,[1,2*] Ricardo Otazo,[2] Arvind Caprihan,[3,4] Juan Bustillo,[1] Hongji Chen,[1] Pierre-Gilles Henry,[5] Malgorzata Marjanska,[5] Charles Gasparovic,[3,6] Chun Zuo,[7] Vincent Magnotta,[8] Bryon Mueller,[5] Paul Mullins,[3] Perry Renshaw,[7] Kamil Ugurbil,[5] Kelvin O. Lim,[5] and Jeffry R. Alger[9]

In this multicenter study, 2D spatial mapping of *J*-coupled resonances at 3T and 4T was performed using short-TE (15 ms) proton echo-planar spectroscopic imaging (PEPSI). Water-suppressed (WS) data were acquired in 8.5 min with 1-cm^3 spatial resolution from a supraventricular axial slice. Optimized outer volume suppression (OVS) enabled mapping in close proximity to peripheral scalp regions. Constrained spectral fitting in reference to a non-WS (NWS) scan was performed with LCModel using correction for relaxation attenuation and partial-volume effects. The concentrations of total choline (tCho), creatine + phosphocreatine (Cr+PCr), glutamate (Glu), glutamate + glutamine (Glu+Gln), *myo*-inositol (Ins), NAA, NAA+NAAG, and two macromolecular resonances at 0.9 and 2.0 ppm were mapped with mean Cramer-Rao lower bounds (CRLBs) between 6% and 18% and ~150-cm^3 sensitive volumes. Aspartate, GABA, glutamine (Gln), glutathione (GSH), phosphoethanolamine (PE), and macromolecules (MMs) at 1.2 ppm were also mapped, although with larger mean CRLBs between 30% and 44%. The CRLBs at 4T were 19% lower on average as compared to 3T, consistent with a higher signal-to-noise ratio (SNR) and increased spectral resolution. Metabolite concentrations were in the ranges reported in previous studies. Glu concentration was significantly higher in gray matter (GM) compared to white matter (WM), as anticipated. The short acquisition time makes this methodology suitable for clinical studies. Magn Reson Med 58:236–244, 2007. © 2007 Wiley-Liss, Inc.

Key words: magnetic resonance spectroscopic imaging; proton echo planar spectroscopic imaging; glutamate; spectral quantification; human brain

Proton magnetic resonance spectroscopic mapping (^{1}H-MRSI) of brain metabolites can identify biomarkers relevant to psychiatric and neurological disease. There is currently increasing interest in extending ^{1}H-MRSI techniques and processing capabilities to map *J*-coupled brain metabolite resonances. Glutamate (Glu) and glutamine (Gln) mapping is of particular interest because these metabolites are key components of energy metabolism and nitrogen homeostasis pathways, and are also involved in excitatory synaptic neurotransmission (1). In vivo mapping of Glu in clinically feasible acquisition times may have important diagnostic applications in psychiatric disorders (2,3) and studies of aging (4).

Thus far, Glu and Gln have been studied mostly by single-voxel MR spectroscopy (MRS) using a variety of techniques, including model-based fitting of short-TE spectra (4–7), use of optimized intermediate TE (8) and Carr-Purcell refocusing pulses (9), spectral editing (10), and 2D *J*-resolved spectroscopy (11,12). MRSI studies of Glu and Gln have used spectral fitting at short TE (13,14), *J*-refocused coherence transfer (15), and, more recently, 2D *J*-resolved spectroscopic imaging (16,17). Spectral editing and 2D *J*-resolved MRSI techniques enable highly selective mapping of Glu and Gln, but they require multistep encoding, which prolongs the acquisition times and limits the sensitivity gains at high field, as metabolite T_2 values have been shown to decrease with field strength (18,19). Short-TE acquisition of single-voxel spectra at high field (4T, 7T, and 9.4T) with constrained spectral fitting and modeling of macromolecular resonances has been shown to provide reliable quantification of a large number of multiplet resonances (5,6,20). It is of interest to extend this approach to MRSI and assess the sensitivity for mapping Glu and other coupled resonances.

Echo-planar and spiral MRSI techniques are increasingly becoming a practical alternative to conventional phase-encoded MRSI (16,17,21). They have comparable SNRs per unit time and unit volume (21–23), and enable high spatial resolution and large volume coverage within a short encoding time, integration of 2D *J*-resolved techniques (16,17), and rapid acquisition of water reference scans. In previous studies we demonstrated the feasibility of short-TE metabolite mapping at 1.5T using the proton echo-planar spectroscopic imaging (PEPSI) technique (21). Recently, we showed that PEPSI provides linear gains in sensitivity with field strengths between 1.5T and 7T (23). However, mapping of multiplet resonances at high field strength using short-TE high-speed MRSI techniques has not yet been demonstrated. This methodology is techni-

[1]Department of Psychiatry, University of New Mexico School of Medicine, Albuquerque, New Mexico, USA.

[2]Department of Electrical and Computer Engineering, University of New Mexico, Albuquerque, New Mexico, USA.

[3]MIND Institute, Albuquerque, New Mexico, USA.

[4]New Mexico Resonance, Albuquerque, New Mexico, USA.

[5]Center for Magnetic Resonance Research, University of Minnesota, Minneapolis, Minnesota, USA.

[6]Department of Neurology, University of New Mexico School of Medicine, Albuquerque, New Mexico, USA.

[7]McLean Hospital Brain Imaging Center, McLean Hospital, Harvard University, MA

[8]Department of Radiology, University of Iowa, Iowa City, Iowa, USA.

[9]Ahmanson-Lovelace Brain Mapping Center, Department of Neurology, David Geffen School of Medicine, University of California–Los Angeles, Los Angeles, California, USA.

Grant sponsor: NIDA; Grant numbers: 1 R01 DA14178-0; P41 RR08079; Grant sponsor: MIND Institute; Grant number: DE-FG02-99ER62764.

*Correspondence to: Stefan Posse, Ph.D, Department of Psychiatry, University of New Mexico School of Medicine, 4200 Tucker NE, Albuquerque, NM 87131. E-mail: sposse@unm.edu

Received 24 November 2006; revised 31 March 2007; accepted 3 April 2007.

DOI 10.1002/mrm.21287

Published online in Wiley InterScience (www.interscience.wiley.com).

cally challenging at high field because 1) limitations in gradient rise times will limit the spectral width at high field (24), which makes spectral fitting difficult due to possible spectral aliasing; and 2) eddy currents due to fast gradient switching cause line-shape distortion, particularly at short TE.

The aim in this multicenter study was to assess the feasibility of 2D spatial mapping of *J*-coupled resonances in the human brain at 3T and 4T using short-TE (15 ms) PEPSI with optimized outer volume suppression (OVS) and a measurement time of less than 10 min. The study was performed at 3T because this field strength is being increasingly used for routine clinical examinations, and at 4T because previous studies using single-voxel techniques have shown the feasibility of quantifying Glu and Gln at this field strength (5,6,20). A spectral quantification pipeline based on LCModel fitting (25) with correction for relaxation and partial-volume effects was developed to assess gray (GM)/white matter (WM) differences in metabolite concentration and to compare sensitivity between the two field strengths.

MATERIALS AND METHODS

Subjects and Scanners

Healthy subjects participated after giving institutionally reviewed informed consent. Data on nine subjects (eight males and one female, age range: 23–42 years, mean: 31 years) were collected on identically equipped Siemens Trio 3T scanners located at the McLean Hospital Brain Imaging Center (three subjects), the University of Iowa Department of Radiology (three subjects) and the University of Minnesota Center for Magnetic Resonance Research (three subjects). Data on nine subjects (six males and three females, age range: 20–45 years, mean: 31 years) were collected on a Bruker MedSpec 4T MR scanner located at the University of New Mexico MIND Imaging Center.

All scanners were equipped with the Siemens Syngo hardware and software platform (VA25) and Sonata gradients (40 mT/m, 200 mT/m/ms slew rate). The 3T scanners were equipped with a circularly polarized (CP) transmit body RF coil and CP receive head coil. The 4T MedSpec scanner was equipped with a transmit/receive CP head coil.

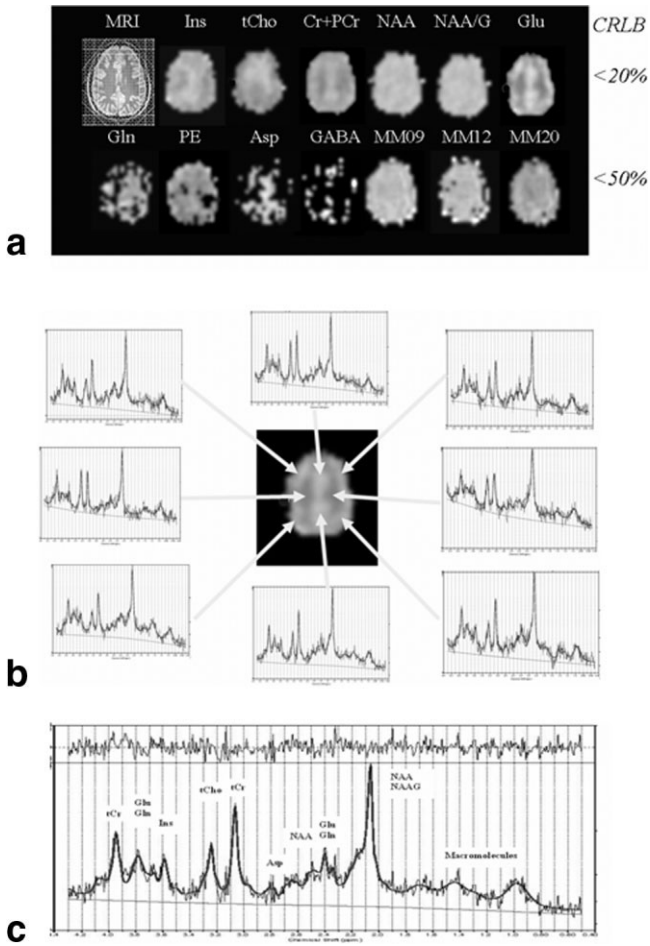

FIG. 1. **a:** Metabolite images and T_2-weighted high-resolution MRI with overlaid OVS slices at 3T show volume coverage for the major metabolites (CRLBs $<$ 20%) and MMs, which extends well into lateral GM areas. The CRLB threshold for voxel selection is shown on the right side. The Glu image shows significantly higher concentration in GM as compared to WM. **b:** Selected 3T spectra with overlaid LCModel fit from peripheral and central brain regions of the data set in **a** in reference to the Glu image demonstrate uniform spectral resolution, a low level of contamination from peripheral lipid signals, and excellent spectral fit quality. The increased Glu multiplet in central and lateral GM as compared to WM, and the macromolecular resonances are clearly delineated. **c:** The selected spectrum from central GM shows the high quality of the LCModel fit.

Pulse Sequence

The main features of the pulse sequence used for this study were recently described (23). The pulse sequence consists of a three-pulse water suppression enhanced through T_1 effects (WET) water suppression module (26), an OVS module using nine-lobe sinc-shaped optimized suppression RF pulses, a spin-echo excitation module with an eight-lobe Hamming-filtered sinc excitation RF pulse (2.6-ms duration, 1.7-kHz bandwidth) and a numerically optimized refocusing RF pulse (27), and an echo-planar readout module. The durations of the suppression and refocusing RF pulses were minimized within the constraints of the available RF amplitude (to less than 5.12 ms). The transmitter frequency of the excitation and refocusing RF pulses was centered at the chemical shift of NAA to minimize chemical-shift displacement artifacts. Spatial-spectral encoding was performed with a train of 1024 alternating 400-μs-long trapezoidal readout gradients using online regridding of the ramp-sampled data and 166.66-kHz acquisition bandwidth. The reconstructed spectral width after even-odd echo editing (see below) was 1086 Hz (8.8 ppm at 3T and 6.4 ppm at 4T) with 2.1-Hz digital spectral resolution. OVS consisted of eight manually prescribed 25–30-mm-thick presaturation slices positioned octagonally along the contours of the brain (Fig. 1) taking into account chemical-shift displacement ($<$5 mm for lipids at 0.9 ppm with respect to water at 4T). The amplitudes of presaturation RF pulses were tuned in vivo for each of the suppression slices in a separate series of calibration experiments in several subjects at 3T and 4T to account for T_1-relaxation effects and B_1 inhomogeneity.

These tuning values were found to be consistent across subjects, resulting in more than 20-fold lipid suppression, and applied to all scans in this study.

Data Acquisition

Data were acquired from axial slices in a supraventricular location using first- and second-order autoshimming and the following parameters: TR = 2 s, TE = 15 ms, FOV = 260 mm, slice thickness = 15 mm, spatial matrix = 32 × 32 pixels, nominal voxel size = 1 cm^3, and scan time = 8.5 min using eight averages. In addition to the water-suppressed acquisition (WS), a non-WS (NWS) reference scan with one average was collected. High-resolution multislice T_2-weighted turbo spin-echo scans with the same slice orientation and T_1-weighted Magnetization Prepared Rapid Gradient Echo (MP-RAGE) scans were acquired for placement of the saturation bands and spatial coregistration. The setup time for manually positioning the OVS slices in three spatial dimensions across the entire MRSI slab based on the high-resolution MRI, autoshimming, and automatic adjustment of the WS pulse amplitudes was 3 min. The total experiment time, including high-resolution imaging, was 18 min.

MRSI Preprocessing and Reconstruction

Data reconstruction was performed as described previously (21,23) using separate processing of odd and even echoes. A sine bell filter was applied across the two *k*-space dimensions to reduce peripheral lipid contamination due to the point spread function (PSF), which increased the effective voxel volume to 1.34 cm^3. Eddy-current correction using Klose's (28) method was applied to the NWS and WS time-domain data using the phase of the NWS data. Each array was then subjected to 3D fast Fourier transform (FFT) reconstruction. Automatic zero-order phase correction and frequency shift correction based on the water signal in the NWS reference scan were applied on a voxel-by-voxel basis. Odd and even spectra were then summed to obtain NWS and WS spectral arrays. Spectra were converted to time-domain by an inverse FT and exported for LCModel fitting using an amplitude threshold to exclude voxels with low SNR originating from regions outside of the brain.

Spectral Fitting

Localized spectra were quantified using LCModel fitting (version 6.1) (25). Simulated basis sets for the pulse sequence parameters used in this study included the following 18 metabolites: aspartate (Asp), choline (Cho), creatine (Cr), gamma-amino-butyric acid (GABA), Gln, glycerophosphocholine (GPC), glutathione (GSH), Glu, *myo*-inositol (Ins), glucose (Glc), lactate (Lac), *N*-acetyl-aspartate (NAA), *N*-acetylaspartylglutamate (NAAG), phosphocholine (PCho), phosphocreatine (PCr), phosphoethanolamine (PE), scyllo-inositol (sIns), and taurine. The following sums were also reported by the fitting program: Cr+PCr, Gln+Glu, and NAA+NAAG. Experimentally, it was found that modeling Cho, PCho, GPC, and the sum Cho+PCho+GPC increased CRLBs as compared to modeling a single Cho component only, which may be due to the similarity of these basis spectra. The most stable fitting results were obtained by fitting GPC only, which thus represents total Cho (tCho) in our analysis. The basis sets for LCModel were generated in Matlab (MathWorks, Natick, MA, USA) by simulating the spectral pattern of each metabolite using density matrix simulations (29). Spectra were simulated based on published chemical-shift and *J*-coupling values (30) with 2-Hz Lorentzian line-broadening.

Lipids (0.9 ppm – Lip09, two resonances at 1.3 ppm – Lip13a – Lip13b, 2 ppm – Lip 20) and macromolecules (MMs; 0.9 ppm – MM09, 1.2 ppm – MM12, 1.4 ppm – MM14, 1.7 ppm MM17, 2.0 ppm – MM20) were simulated using default settings of LCModel 6.1, which include soft constraints for peak position and line width, and prior probabilities of the ratios of MM and lipid peaks.

Spectra were fitted in the spectral range between 0.2 and 4.2 ppm in reference to the NWS data using "water-scaling." Two Cramer-Rao lower bound (CRLB) thresholds were used in this study: <20% = excellent reliability, and <50% = acceptable reliability.

The following metabolites were included in the analysis of spectroscopic images, since their CRLBs in most of the voxels within the volume of interest were less than 50%: Ins, tCho, Cr+PCr, NAA, NAA+NAAG, Glu, Glu+Gln, PE, MM09, MM12, MM20, GSH, GABA, Gln, and Asp. Other metabolites and lipids were fitted with much higher CRLBs. Voxels were included if 1) CRLB < 20% for Ins, tCho, Cr+PCr, NAA, NAA+NAAG, Glu, Glu+Gln, MM09, MM12, and CRLB < 50% for PE, MM20, GSH, GABA, Gln, and Asp; and 2) if the estimated singlet line width of the LCModel fit was smaller than 0.1 ppm.

Relaxation and Partial-Volume Correction

High-resolution T_1 and T_2 images were segmented into cerebrospinal fluid (CSF), GM, and WM maps, resampled, and filtered using the FAST and FLIRT routines implemented in FSL (www.fmrib.ox.ac.uk/fsl/) to match the PSF, slice thickness, and FOV of the PEPSI data. The resulting low-resolution maps of GM, WM, and CSF were converted into water concentration maps $[H_2O_{GM,v}]$,$[H_2O_{WM,v}]$,$[H_2O_{CSF,v}]$ that were corrected for the concentration of MR visible water in the three compartments using literature values reported by Ernst et al. (31).

The relaxation attenuation of water and metabolites signals was computed as:

$$Att = S(TE,TR)/S_o = e^{TE/T_2} * (1 - e^{TR/T_1}) \qquad [1]$$

where S_0 is the fully relaxed signal. T_1 and T_2 values in different tissue compartments taken from the literature (16,18,32–36) are listed in Table 1. The T_1-value for Glu was assumed to be the same as for tCho, based on Srinivasan et al. (16) who reported similar T_1 values for Cho and Glu, and on a recent study in rat cortex (36). In accordance with a study by Hetherington et al. (19) the T_1 and T_2 values of metabolites at 4T for GM and WM were assumed to be similar. The relaxation times of Ins at 4T were assumed to be similar to that of tCho based on Ethofer et al. (32). The T_1 values of MM resonances at 3T and 4T were assumed to be 300 ms and 350 ms, respectively, based on

Table 1
T_1 and T_2 Values for Relaxation Correction Taken From the Literature

	GM (ms)		WM (ms)		CSF (ms)		Reference #
	T_1	T_2	T_1	T_2	T_1	T_2	
3 T							
Water	1470	110	1060	74	3000	200	32,34
tCho	1250	222	1210	222			32,33
Cr + PCr	1330	162	1400	178			32,33
Gln, Glu	1250	200	1210	200			16
Ins	1120	200	960	200			32,33
NAA, NAAG	1470	247	1560	301			32,33
MM09, MM12, MM20	300	44	300	44			37
4 T							
Water	1500	63	1000	50	4000	200	35
tCho	1290	179	1290	179			18
Cr + PCr	1720	141	1720	141			18
Gln, Glu	1290	179	1290	179			16,36
Ins	1290	179	1290	179			
NAA, NAAG	1630	230	1630	230			18
MM09, MM12, MM20	350	44	350	44			37

Ref. 37, taking into account a slight increase in T_1 with field strength (36). The T_2 values of the MM resonances were assumed to be 44 ms based on Ref. 37.

Relaxation- and partial-volume-corrected metabolite concentrations in units of [mmol/l] were computed on a voxel-by-voxel basis using Eq. [8] in Ref. 38 with a modification that allows for GM/WM differences in metabolite relaxation:

$$[\mathrm{metab}]_{\mathrm{corr}} = \frac{[\mathrm{metab}]_{\mathrm{LCModel}} * \mathrm{f} * \{[H_2O_{GM,v}] * \mathrm{Att}_{\mathrm{H_2O,GM}} + [H_2O_{WM,v}] * \mathrm{Att}_{\mathrm{H_2O,WM}} + [H_2O_{CSF,v}] * \mathrm{Att}_{\mathrm{H_2O,CSF}}\}}{[\mathrm{H_2O_{GM,v}}] * \mathrm{Att}_{\mathrm{Met,GM}} + [H_2O_{WM,v}] * \mathrm{Att}_{\mathrm{Met,WM}}} \quad [2]$$

where

$$f = \frac{35.880 * (1.21 * [H_2O_{GM}] + [H_2O_{WM}])}{55.555 * ([H_2O_{GM}] + [H_2O_{WM}])} \quad [3]$$

The concentration values of PE, GSH, GABA, Gln, and Asp were corrected for water relaxation attenuation but not for metabolite relaxation attenuation, due to a lack of reported metabolite T_1 and T_2 values in human brain.

The means and standard deviations (SDs) across the MRSI slice were computed for metabolite concentrations, CRLBs, singlet line width, and SNR. The volume of voxels above threshold (sensitive volume) was computed for each resonance. The statistical regression method of Hetherington et al. (39) was used to estimate the concentration in pure GM and WM.

RESULTS

Metabolite Images and Spectra

Figure 1a shows representative metabolite images obtained at 3T and the corresponding high-resolution MRI with overlaid OVS bands. The images of Ins, tCho, Cr+PCr, NAA, NAA+NAAG, Glu, and MMs demonstrate mapping across the entire slice, including lateral GM areas. The Glu image shows similar intensity in central and lateral GM, and much lower intensity in WM, consistent with previous studies (13–17). The images of the macromolecular peaks at 0.9, 1.2 and 2.0 ppm display similar intensity in central and peripheral regions, which suggests that contamination from peripheral lipid-containing regions was small. The images of Gln, PE, Asp, and GABA are limited by SNR and show signal voids, where the CRLBs exceed 50%. Figure 2b shows spectra sampled from several voxel locations in central and lateral regions with clearly delineated macromolecular resonances and only small lipid contamination. The smooth fitted baseline in these data is typical for results at 3T. Figure 2c shows the excellent fit quality obtained in a representative spectrum from central GM.

Figure 2a shows representative metabolite images obtained at 4T. The volume coverage for mapping Ins, tCho, Cr+PCr, NAA, NAA+NAAG, Glu, and MMs is similar to that at 3T. Reduced areas with signal voids due to the increased sensitivity at 4T are seen in the Gln, PE, Asp, and GABA images. Figure 2b shows spectra sampled from several voxel locations, including lateral GM, with uniform spectral quality and only minor lipid contamination. The baseline in these spectra is slightly more modulated as compared to 3T with broad humps in the spectral ranges of 2.2 and 3.8 ppm. The spectral quality (Fig. 2c) is similar to that obtained with single-voxel techniques at this field strength (e.g., Fig. 9 in Ref. 20).

Sensitivity and CRLBs

The average SNR of the LCModel fit at 4T (9.2 ± 0.9) was significantly higher than at 3T (6.9 ± 1.0, t = 5.07, df = 16, $P < 0.00012$). The estimated singlet line width in units of ppm at 4T (0.041 ± 0.003 ppm) was significantly narrower than at 3T (0.048 ± 0.005 ppm, t = 3.52, df = 16, $P <$

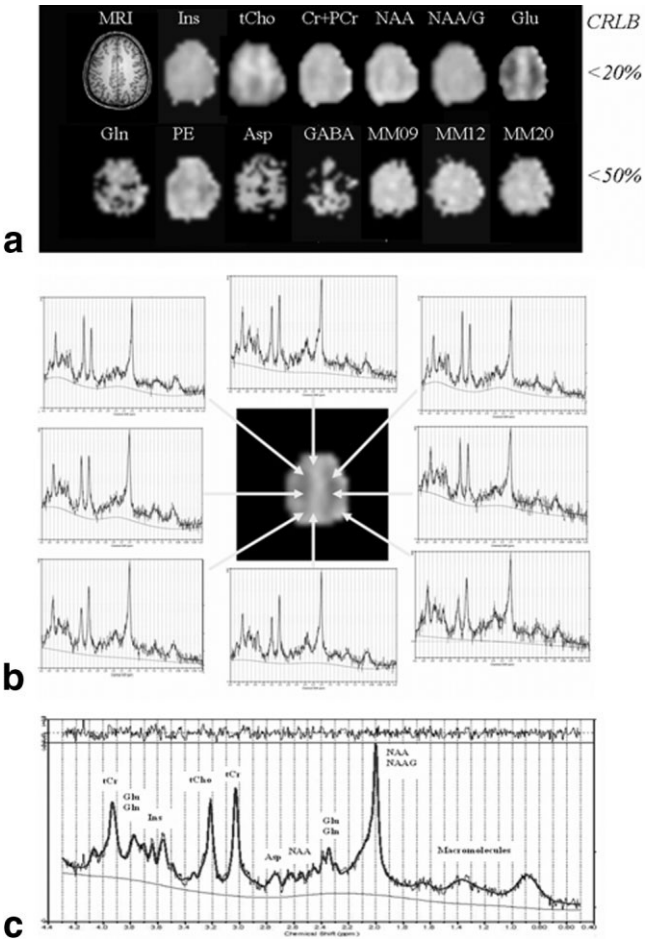

FIG. 2. **a:** Metabolite images at 4T with corresponding high-resolution MRI show a volume coverage in lateral GM for the major metabolites (CRLBs < 20%) and MMs that is comparable to that at 3T. Improved volume coverage is seen for Gln, PE, GABA, and Asp. **b:** Selected spectra at 4T with overlaid LCModel fit from peripheral and central brain regions of the data set in **a** in reference to the Glu image show similar spectral quality as compared to 3T, and a low degree of lipid contamination. **c:** Selected spectrum from central GM with overlaid LCModel fit shows clearly resolved multiplet peaks around 2.35 ppm.

0.0029), which is consistent with previous studies that compared spectral resolution across field strength (5,23).

Highly reliable fits with mean CRLBs below 10% were obtained for Cr+PCr, NAA, and NAA+NAAG at both field strengths. Good fits with mean CRLBs below 18% were obtained for tCho, Glu, Glu+Gln, Ins, MM09, and MM20. Acceptable fit reliability was obtained for low concentration *J*-coupled resonances of Asp, GABA, Gln, GSH, and PE, and for the MM12 resonance with mean CRLBs between 30% and 44%. The mean CRLBs of most metabolites, with the exception of Gln, Glu+Gln, MM09, MM12, and PE, were significantly lower at 4T vs. 3T (Fig. 3a), $t > 2.58$, $df = 16$, $P < 0.02$. The average decrease of the CRLBs was 19%.

The sensitive volumes of Cr+PCr, NAA, and NAA+NAAG were between 169 cm^3 and 182 cm^3, and differed less than 5% between field strengths. The sensitive volume of tCho was larger at 4T (152 ± 26 cm^3) as compared to 3T (117 ± 42 cm^3). The sensitive volumes of Glu, Glu+Gln, and Ins were between 147 cm^3 and 162 cm^3, and differed less than 10% between field strengths. Strong increases of the sensitive volume with field strength were measured for Asp (mean: 1.7-fold), GABA (mean: 4.9-fold), and GSH (mean: 1.7-fold).

Metabolite Concentration Values

Figure 3b shows slice-averaged concentration values at 3T and 4T, which are within the range of concentration values reported in previous studies at these field strengths (6–8,11,13–17,20,40–42). Differences in mean concentration values between the two field strengths were less than 23%, with the exception of Gln (34%). These differences were statistically significant for Cr+PCr, NAA, NAA+NAAG, Glu, Glu+Gln, PE, MM20, and Gln ($t > 2.3$, $df = 16$, $P < 0.04$). Within each field strength the mean concentration values had an SD across subjects of less than 20%, with the exception of MM12 (22%) and Gln at 4T (38%). Figure 4a shows extrapolated pure WM and GM concentration values of Ins, tCho, Cr+PCr, Glu, Glu+Gln, Ins, NAA, NAA+NAAG, MM09, and MM20 at 3T. The strongest GM/WM contrast was measured for Glu (concentration ratio: 1.9 ± 0.4) and Glu+Gln (concentration ratio: 1.8 ± 0.4). The extrapolated GM/WM contrast was slightly higher at 4T (Fig. 4b), but that difference was not statistically significant except for tCho ($t > 3.23$, $df = 16$, $P < 0.0053$). The strongest GM/WM contrast was measured for Glu (concentration ratio: 2.6 ± 0.9) and Glu+Gln (concentration ratio: 2.4 ± 0.7). The GM/WM contrast of MM09 and MM20 was similar at both field strengths.

An estimate of the reproducibility of metabolite concentrations was obtained in the three subjects measured at 3T

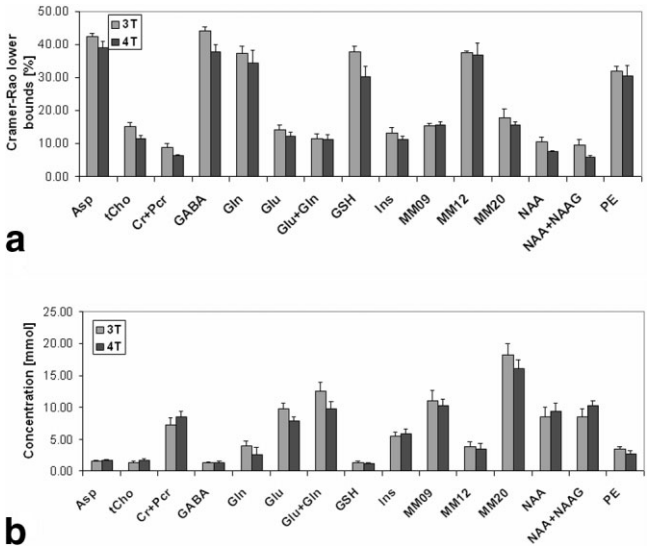

FIG. 3. **a:** Mean CRLBs of the LCModel fit were smaller at 4T as compared to 3T for most metabolites, with the exception of Gln, Glu+Gln, MM09, MM12, and PE (*:$t > 2.58$, $df = 16$, $P < 0.02$). This decrease reflects the expected sensitivity increase with field strength. **b:** Mean metabolite concentration values, averaged across the slice, were similar at 3T and 4T, and in the range of concentration values reported in previous studies at these field strengths.

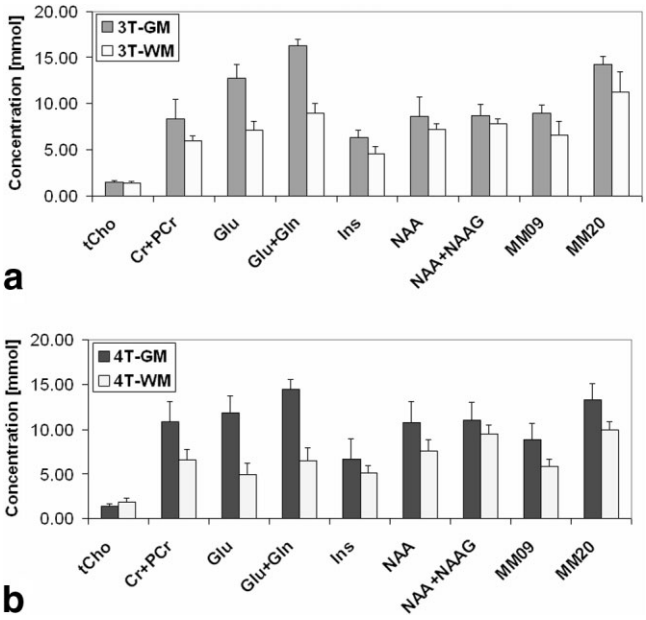

FIG. 4. Extrapolated pure GM and WM metabolite concentration values at (**a**) 3T and (**b**) 4T. The largest GM/WM contrast was measured for Glu and Glu+Gln, as expected.

at the University of Minnesota. The within-session variation was less than 12% for all metabolites. Metabolite concentrations measured on different days in one of the three subjects varied by less than 10%.

DISCUSSION

Data Acquisition

This study demonstrates the feasibility of quantitative whole-slice mapping of *J*-coupled resonances at 3T and 4T with the PEPSI high-speed MRSI technique. We used a much shorter TE than that typically used for MRSI, since preliminary measurements on three subjects at 4T showed a twofold increase of the sensitive volume of Glu when the TE was decreased from 30 to 15 ms ($t = 5.95$, $df = 4$, $P < 0.004$).

The spectral width of the PEPSI method is adequate for encoding the entire range of metabolites visible at short TE. The amide protons of NAA and other peaks in the vicinity of 8 ppm wrap around to the right of NAA and do not interfere with spectral fitting. Correction for frequency drifts due to shim heating effects was not applied in this study, since drifts were on the order of 1–3 Hz, which is considerably smaller than the intrinsic spectral line width in vivo. In a previous study, at a higher spatial resolution (not used in the present study), these frequency drifts did become significant, and we developed an online frequency correction for the water-suppression pulses and used separate acquisition of individual averages to minimize incoherent averaging due to frequency drifts (43).

The placement and optimization of the thickness of the eight OVS slices was time-consuming and required skill and experience to balance the need to adequately suppress peripheral areas and minimize suppression of cortical regions. Since different operators acquired the data, there was a slight variability in lipid suppression between subjects, but the capability of LCModel to fit lipid signals using "soft constraints" compensated for small lipid contamination, and the metabolite maps in these subjects did not show significant degradation in peripheral areas. To overcome this limitation we are currently developing automatic positioning of the saturation bands, which is desirable for clinical studies and virtually indispensable when positioning larger number of OVS slices for 3D volumetric coverage (44).

Spectral Fitting

The performance of spectral fitting is sensitive to spectral line width, SNR, and the choice of fitting parameters. Lateral GM spectra suffer susceptibility-related line broadening, and CRLBs increase accordingly. More reliable comparisons when averaging fitting results over the slice could be obtained by removing peripheral voxels and using a lower threshold for spectral line width, at the expense of reducing the sensitive volume.

The ability of the baseline fit to account for errors in modeling MMs and residual lipids improves with increasing SNR, as described by Pfeuffer et al. (5). Spectra with flat baselines can yield more reproducible (but consistently wrong) results, with deceptively low coefficients of variation (5). The flat baseline in our 3T data suggests that they are more strongly SNR-limited than our 4T data. Using multivoxel averaging of individual voxel spectra at 3T, we confirmed that increasing SNR increases the modulation of the baseline and reduces the overestimation of the Glu concentration, which makes 3T and 4T results similar.

We also investigated whether constraining the model for macromolecular peaks using experimentally measured metabolite-nulled spectra from a recent study (23) would improve the fit quality. The mean CRLBs increased slightly as compared to default modeling of MMs, while the fitted metabolite concentrations were similar except for a slight decrease in NAA and Glu concentration. This suggests that LCModel can adequately account for macromolecular signals using default parameters for modeling MMs. However, appropriate modeling of the MM resonances in clinical scans in diseased brain may require direct measurement of metabolite-suppressed MM spectra.

Metabolite Quantification

Our CRLB data show that spectral quantification is more robust at 4T as compared to 3T, which is consistent with the increased spectral dispersion, the 16% reduction in singlet line width (in ppm), and the 33% increase in singlet SNR at 4T. The measured Glu and Gln concentrations at 4T were lower than at 3T, while the measured NAA concentration was higher, which may be explained by the reduced spectral overlap and increased SNR at 4T. To further examine the SNR dependence of the LCModel fit results, we performed a separate series of experiments at 4T using different numbers of signal averages (data not shown) and found that the measured Glu and Glu concentrations indeed decreased with increasing SNR. It is thus not surprising that the measured metabolite concentration

Table 2
Comparison of Metabolite Concentration Values in Units of mmol/L (SD) in Different Studies

Study	B_0 [T]	Method	tCho		Cr+PCr		Glu		Ins		NAA	
			GM	WM	GM	WM	GM	WM	GM	WM	GM	WM
Schubert 2004 (8)	3	SVS - TE 80 ms					11.6 (1.4)					
Hurd 2004 (11)[a]	3	SVS - TE averaged	1.3 (0.1)	1.8 (0.1)	7.6 (0.8)	5.9 (0.5)	12.3 (1.1)	7.5 (0.5)			10.0 (0.7)	7.4 (0.4)
Srinivasan 2006 (16)	3	MRSI - TE averaged	1.8 (0.6)	1.5 (0.1)	9.7 (0.9)	6.2 (0.9)	9.4 (1.0)	4.5 (0.6)	7.7 (0.9)	4.3 (0.5)	10.4 (0.8)	8.5 (1.0)
Present study	3	MRSI - TE 15 ms	1.4 (0.2)	1.4 (0.2)	8.4 (0.9)	6.0 (0.5)	12.8 (1.5)	7.0 (1.1)	6.3 (0.7)	4.6 (0.7)	8.6 (0.7)	7.2 (0.7)
Hetherington 1996 (39)	4.1	MRSI - TE 50 ms	1.5 (0.3)	1.5 (0.2)	8.2 (0.5)	6.1					9.7 (1.1)	10.5 (0.6)
Pan 1998 (40)	4.1	MRSI - TE 50 ms	1.6 (0.5)	1.8 (0.2)	8.8 (1.6)	6.2 (0.8)					9.4 (0.9)	11.1 (0.9)
Kassem 2003 (7)	4	SVS - TE 46 ms		2.2 (0.3)		7.4 (0.8)		5.5 (0.5)		5.6 (0.7)		9.4 (1.0)
Tkac 2005 (20)[a]	4	SVS - TE 4 ms	1.3		9.1		10.1		6.8		11.2	
McNab 2006 (14)	4	MRSI - TE 46 ms		3.1 (0.5)		9.8 (2.1)		7.8 (2.2)		8.1 (2.3)		12.6 (1.8)
Present study	4	MRSI - TE 15 ms	1.4 (0.3)	1.8 (0.4)	10.9 (1.8)	6.6 (1.1)	11.9 (1.9)	5.0 (1.2)	6.7 (1.1)	5.1 (0.9)	10.8 (2.3)	7.6 (1.3)

[a]Values were converted from mmol/kg to mmol/L using a correction factor of 1.04 (47).
SVS = single voxel spectroscopy, MRSI = MR spectroscopic imaging.

values at 3T and 4T in this study are slightly different due to our study design, which is associated with a lower SNR compared to that in previous single-voxel studies (20). The use of tight-fitting phased-array surface RF coils would significantly increase sensitivity in both peripheral and central brain regions. We thus expect that metabolite concentrations measured at 3T and 4T with high-speed MRSI and phased-array coils will be consistent with previous single-voxel studies demonstrating comparable spectral quantification across field strengths (20).

Partial-volume correction is sensitive to the choice of segmentation method (38), to larger B_1-inhomogeneity at 4T, and to differences in image contrast between field strengths. These can introduce bias in the segmentation and the extrapolated metabolite concentrations in "pure" GM and WM, which may contribute to the differences in measured metabolite concentration values at 3T and 4T. Relaxation correction is sensitive to errors in T_1 values, in particular for CSF. For clinical studies it would thus be advantageous to measure metabolite and water T_1 in individual subjects to limit possible errors in relaxation correction. Alternatively, it is possible to conduct studies at longer TR values to limit the effects of T_1 relaxation.

Table 2 shows a comparison of tCho, Cr+PCr, Glu, Ins, and NAA concentrations reported in selected studies at 3T and 4T using either spectral fitting or TE averaging. The data in these studies were corrected for T_1 relaxation or measured at long TR. The TE-averaged data in Ref. 16 were not corrected for T_2 relaxation of Glu and thus underestimate the Glu concentration. This underestimation may be as high as 40%, assuming a T_2 of Glu in GM on the order of 200 ms, as reported by Schubert et al. (8). With this T_2 correction the Glu concentration in the Srinivasan et al. (16) study would be in the range of the other studies. The concentration of Glu in our 3T data is consistent with that in the *J*-resolved studies and the study by Schubert et al. (8). The Glu concentration in our 4T data is consistent within 10% with previous studies by Tkac and Gruetter (20) and Kassem and Bartha (7).

Several metabolites showed distinct GM/WM contrast, including Glu, Glu+Gln, and Cr+PCr. The strong GM/WM contrast of Glu in this study is consistent with previous studies (e.g., Ref. 16). The larger GM/WM contrast in tCho at 4T as compared to 3T can in part be explained by the larger sensitive volume of tCho at 4T, which includes a larger number of lateral GM voxels.

A number of low-concentration *J*-coupled resonances, such as Asp, GABA, GSH, Gln, and PE, were detected with greater sensitivity at 4T as compared to 3T. These were quantified without correction for metabolite T_1 relaxation effects and thus underestimated. The CRLBs in individual voxels were relatively large, but averaging across the entire slice resulted in concentration values that are in the range of previously reported values. The Asp concentrations in this study were 1.6 mmol/l at 3T and 1.7 mmol/l at 4T compared to 2.1 mmol/l in Ref. 20 and 3.2 mmol/l in Ref. 7. The GABA concentrations in this study were 1.3 mmol/l at 3T and 4T compared to 0.8 mmol/l in Refs. 20 and 41. The Gln concentration in this study was 2.7 mmol/l compared to 3.4 mmol/l in Ref. 20, 3.0 mmol/l in Ref. 10, and 2.6 mmol/l in Ref. 11. The GSH concentration in this study was 1.2 mmol/l compared to 1.3 mmol/l in Ref. 45,

0.8 mmol/l in Ref. 20, and 2–5 mmol/l in Refs. 10 and 42. However, the PE was higher in this study with 3.5 mmol/l at 3T and 2.7 mmol/l at 4T compared to 1.8 mmol/l in Ref. 20. Improved quantification of these *J*-coupled metabolites is expected using a longer scan time, larger voxel size, and sensitive surface coil arrays.

In addition to metabolites contained in the basis sets, we obtained good fits for MMs at 0.9 and 2.0 ppm, which were fully relaxed due to their short T_1 values and uniformly distributed in GM and WM, consistent with the study by Hwang et al. (46). This feasibility of mapping MM resonances into lateral GM is of interest for clinical applications in multiple sclerosis, stroke, traumatic brain injury, vascular disease, and brain tumors.

CONCLUSIONS

The short acquisition time (<10 min) makes this methodology suitable for clinical studies. In future work we will characterize intra- and intersubject reliability within and across site sites to determine its reliability and robustness for clinical studies. Improvements in sensitivity using large-scale surface coil arrays and higher field strength, more constraint spectral fitting using directly measured macromolecular basis sets, and improved tissue segmentation will make this methodology applicable for identifying and mapping metabolic biomarkers in a wide range of neurological and psychiatric disorders.

ACKNOWLEDGMENTS

The authors thank Ranee Barrow, Rosabelle DeNoi, Donner Holten, Diana South, and Jing Xu (MIND Imaging Center) for help with scanning and subject recruitment, and for software support. We thank Dr. Stephen Provencher and Dr. Gregory J. Moore (Wayne State University) for advice on spectral fitting and for providing comparative LCModel basis sets. We acknowledge the generous technical support of Dr. Stefan Roell and Dr. John Grinstead (Siemens Medical Solutions). We gratefully acknowledge Dr. Nancy C. Andreasen (University of Iowa) for supporting this study.

REFERENCES

1. Shulman RG, Rothman DL, Behar KL, Hyder F. Energetic basis of brain activity: implications for neuroimaging. Trends Neurosci 2004;27:489–495.
2. Coyle JT, Tsai G, Goff DC. Ionotropic glutamate receptors as therapeutic targets in schizophrenia. Curr Drug Targets CNS Neurol Disord 2002;1:183–189.
3. Sanacora G, Gueorguieva R, Epperson CN, Wu YT, Appel M, Rothman DL, Krystal JH, Mason GF. Subtype-specific alterations of gamma-aminobutyric acid and glutamate in patients with major depression. Arch Gen Psychiatry 2004;61:705–713.
4. Kaiser LG, Schuff N, Cashdollar N, Weiner MW. Age-related glutamate and glutamine concentration changes in normal human brain: 1H MR spectroscopy study at 4 T. Neurobiol Aging 2005;26:665–672.
5. Pfeuffer J, Tkac I, Provencher SW, Gruetter R. Toward an in vivo neurochemical profile: quantification of 18 metabolites in short-echo-time 1H NMR spectra of the rat brain. J Magn Reson 1999;141:104–120.
6. Bartha R, Drost DJ, Menon RS, Williamson PC. Comparison of the quantification precision of human short echo time (1)H spectroscopy at 1.5 and 4.0 Tesla. Magn Reson Med 2000;44:185–192.
7. Kassem MN, Bartha R. Quantitative proton short-echo-time laser spectroscopy of normal human white matter and hippocampus at 4 Tesla incorporating macromolecule subtraction. Magn Reson Med 2003;49:918–927.
8. Schubert F, Gallinat J, Seifert F, Rinneberg H. Glutamate concentrations in human brain using single voxel proton magnetic resonance spectroscopy at 3 Tesla. NeuroImage 2004;21:1762–1771.
9. Soher BJ, Pattany PM, Matson GB, Maudsley AA. Observation of coupled 1H metabolites resonances at long TE. Magn Reson Med 2005;53:1283–1287.
10. Choi C, Coupland NJ, Bhardwaj PP, Malykhin N, Gheorghiu D, Allen PS. Measurement of brain glutamate and glutamine by spectrally-selective refocusing at 3 Tesla. Magn Reson Med 2006;55:997–1005.
11. Hurd R, Sailasuta N, Srinivasan R, Vigneron DB, Pelletier D, Nelson SJ. Measurement of brain glutamate using TE-averaged PRESS at 3T. Magn Reson Med 2004;51:435–440.
12. Mayer D, Spielman DM. Detection of glutamate in the human brain at 3 T using optimized constant time point resolved spectroscopy. Magn Reson Med 2005;54:439–442.
13. Mason GF, Pan JW, Ponder SL, Twieg DB, Pohost GM, Hetherington HP. Detection of brain glutamate and glutamine in spectroscopic images at 4.1 T. Magn Reson Med 1994;32:142–145.
14. McNab JA, Bartha R. Quantitative short echo-time (1)H LASER-CSI in human brain at 4T. NMR Biomed 2006;19:999–1009.
15. Pan JW, Mason GF, Pohost GM, Hetherington HP. Spectroscopic imaging of human brain glutamate by water-suppressed *J*-refocused coherence transfer at 4.1 T. Magn Reson Med 1996;36:7–12.
16. Srinivasan R, Cunningham C, Chen A, Vigneron D, Hurd R, Nelson S, Pelletier D. TE-averaged two-dimensional proton spectroscopic imaging of glutamate at 3 T. Neuroimage 2006;30:1171–1178.
17. Mayer D, Kim DH, Adalsteinsson E, Spielman DM. Fast CT-PRESS-based spiral chemical shift imaging at 3 Tesla. Magn Reson Med 2006;55:974–978.
18. Posse S, Cuenod CA, Risinger R, Le Bihan D, Balaban RS. Anomalous transverse relaxation in 1H spectroscopy in human brain at 4 Tesla. Magn Reson Med 1995;33:246–252.
19. Hetherington HP, Mason GF, Pan JW, Ponder SL, Vaughan JT, Twieg DB, Pohost GM. Evaluation of cerebral gray and white matter metabolite differences by spectroscopic imaging at 4.1T. Magn Reson Med 1994;32:565–571.
20. Tkac I, Gruetter R. Methodology of 1H NMR spectroscopy of the human brain at very high fields. Appl Magn Reson 2005;29:139–157.
21. Posse S, Tedeschi G, Risinger R, Ogg R, Bihan DL. High speed 1H spectroscopic imaging in human brain by echo planar spatial-spectral encoding. Magn Reson Med 1995;33:34–40.
22. Pohmann R, von Kienlin M, Haase A. Theoretical evaluation and comparison of fast chemical shift imaging methods. J Magn Reson 1997;129:145–160.
23. Otazo R, Mueller B, Ugurbil K, Wald LL, Posse S. Signal-to-noise ratio and spectral line width improvements between 1.5 and 7 Tesla in proton-echo-planar-spectroscopic-imaging (PEPSI). Magn Reson Med 2006;56:1200–1210.
24. Ebel A, Maudsley AA, Weiner MW, Schuff N. Achieving sufficient spectral bandwidth for volumetric (1)H echo-planar spectroscopic imaging at 4 Tesla. Magn Reson Med 2005;54:697–701.
25. Provencher SW. Automatic quantitation of localized in vivo 1H spectra with LCModel. NMR Biomed 2001;14:260–264.
26. Ogg RJ, Kingsley PB, Taylor JS. WET a T1–B1-insensitive water suppression method for in vivo localized 1H NMR spectroscopy. J Magn Reson Ser B 1994;104;1–10.
27. Mao J, Mareci TH, Andrew ER. Experimental study of optimal selective radiofrequency pulses. J Magn Reson 1988;79:1–10.
28. Klose U. In vivo proton spectroscopy in presence of eddy currents. Magn Reson Med 1990;14:26–30.
29. Henry P-G, Marjanska M, Walls JD, Valette J, Gruetter R, Ugurbil K. POCE NMR spectroscopy in strongly coupled systems. Magn Reson Med 2006;55:250–257.
30. Govindaraju V, Young K, Maudsley AA. Proton NMR chemical shifts and coupling constants for brain metabolites. NMR Biomed 2000;13:129–153.
31. Ernst T, Kreis R, Ross BD. Absolute quantitation of water and metabolites in the human brain. I. Compartments and water. J Magn Reson B 1993;102:1–8.

32. Ethofer T, Mader I, Seeger U, Helms G, Erb M, Grodd W, Ludolph A, Klose U. Comparison of longitudinal metabolite relaxation times in different regions of the human brain at 1.5 and 3 Tesla. Magn Reson Med 2003;50:1296–1301.
33. Traber F, Block W, Lamerichs R, Gieseke J, Schild HH. 1H metabolite relaxation times at 3.0 tesla: measurements of T_1 and T_2 values in normal brain and determination of regional differences in transverse relaxation. J Magn Reson Imaging 2004;19:537–545.
34. Wansapura JP, Holland SK, Dunn RS, Ball Jr WS. NMR relaxation times in the human brain at 3.0 Tesla. J Magn Reson Imaging 1999;9:531–538.
35. Jezzard P, Duewell S, Balaban RS. MR relaxation times in human brain: measurement at 4 T. Radiology 1996;199:773–779.
36. de Graaf RA, Brown PB, McIntyre S, Nixon TW, Behar KL, Rothman DL. High magnetic field water and metabolite proton T_1 and T_2 relaxation in rat brain in vivo. Magn Reson Med 2006;56:386–394.
37. Behar KL, Rothman DL, Spencer DD, Petroff OAC. Analysis of macromolecule resonances in 1H NMR spectra of human brain. Magn Reson Med 1994;32:294–302.
38. Gasparovic C, Song T, Devier D, Bockholt HJ, Caprihan A, Mullins PG, Posse S, Jung RE, Morrison LA. Use of tissue water as a concentration reference for proton spectroscopic imaging. Magn Reson Med 2006;55: 1219–1226.
39. Hetherington HP, Pan JW, Mason GF, Adams D, Vaughn MJ, Twieg DB, Pohost GM. Quantitative 1H spectroscopic imaging of human brain at 4.1 T using image segmentation. Magn Reson Med 1996;36:21–29.
40. Pan JW, Twieg DB, Hetherington HP. Quantitative spectroscopic imaging of the human brain. Magn Reson Med 1998;40:363–369.
41. Jensen JE, Frederick BD, Wang L, Brown J, Renshaw PF. Two-dimensional, *J*-resolved spectroscopic imaging of GABA at 4 Tesla in the human brain. Magn Reson Med 2005;54:783–788.
42. Trabesinger AH, Weber OM, Duc CO, Boesiger P. Detection of glutathione in the human brain in vivo by means of double quantum coherence filtering. Magn Reson Med 1999;42:283–289.
43. Li T, Mullins P, Posse S. Real-time compensation for B_0 field drift in proton echo planar spectroscopic imaging improves water suppression efficiency. In: Proceedings of the 13th Annual Meeting of ISMRM, Miami Beach, FL, USA, 2005 (Abstract 2526).
44. Li T, Martinez-Ramon M, Heileman G, Posse S. Automatic outer volume suppression (OVS) slice placement for proton-echo-planar-spectroscopic-imaging (PEPSI). In: Proceedings of the 14th Annual Meeting of ISMRM, Seattle, WA, USA, 2006 (Abstract 3086).
45. Terpstra M, Henry PG, Gruetter R. Measurement of reduced glutathione (GSH) in human brain using LCModel analysis of difference-edited spectra. Magn Reson Med 2003;50:19–23.
46. Hwang JH, Graham GD, Behar KL, Alger JR, Prichard JW, Rothman DL. Short echo time proton magnetic resonance spectroscopic imaging of macromolecule and metabolite signal intensities in the human brain. Magn Reson Med 1996;35:633–639.
47. Alger JR, Symco SC, Bizzi A, Posse S, DesPres DJ, Armstrong MR. Absolute quantitation of short-TE brain 1H-MR spectra and spectroscopic imaging data. J Comput Assist Tomogr 1993;17:191–199.